shown for comparison. It is not possible to generate the dispersion profile of ASiNR by folding that of 2D Si, but the pattern is similar to that found in nanotube dispersion profiles obtained by zonefolding.[28] In the phonon dispersion profile of hydrogen saturated ASiNR-9 all modes are real, except for some small imaginary frequencies calculated for the twisting acoustic mode, TW, near the Γ point. This issue was faced earlier and was attributed to the limitations of the computational precision.[29] Thus, the structure is predicted to be stable. Computational cost of this calculation is very high, so we were not able to calculate the phonon dispersions for other ribbons. Nevertheless, all ASiNRs have very similar atomic configuration, and thus they are also expected to be stable. The phonon dispersion profile of 2D Ge is similar to that of Si.[16] But in Ge structure the acoustic and optic modes are well separated. Also due to softer bonds the wavenumbers of Ge structure is halved compared to Si. Thus AGeNRs are also expected to be stable, whilst exhibiting the mentioned differences.

Phonon densities of states (DOS) of hydrogen saturated ASiNR-9 projected to atoms at different locations in the nanoribbon are presented in Fig. 2(b). Shown is also DOS of the 2D Si honeycomb structure in the same figure. DOS projected on Si atoms at the center of the nanoribbon is very similar to that of the 2D Si. As the width of the nanoribbon increases, this similarity is expected to be enhanced. However, DOS projected on Si atoms at the edges deviate from that corresponding to 2D Si. Especially, four optical peaks above 600 cm^{-1} are clearly originating from Si-H bonds at the edges. Also modes originating from short Si-Si bonds at the edges cause changes in DOS below 600 cm^{-1}.

IV. ELECTRONIC STRUCTURE

In this section, we investigate the electronic structure of hydrogen saturated Si and Ge nanoribbons. Nanoribbons having widths from $n = 3$ to 30 were investigated. Figure 3 presents the variation of energy gaps and effective masses with the ribbon width given in terms of n. Band gaps are direct and located at the Γ. One can see three branches with decaying profiles originating from the quantum size effect. Here in ascending order of the band gaps, we would like to name these branches with widths $n = 3k+2$, $3k$, and $3k+1$ as family I, II, and III, respectively, where k is an integer. This "family behavior" was also observed in armchair graphene nanoribbons.[20] This trend is explained by foldings of infinite graphene band profile, which is easily understood by using a tight binding model. The simplest possible model is to assume that only the first nearest neighbors interact and have equal hopping parameters with self-energies set to zero. But this model results in zero band gap for the members of the family I. Fortunately, this problem is fixed if a different parameter is used at the edges.[20] As we mentioned in the previous section, the Si-Si (and Ge-Ge) bond length

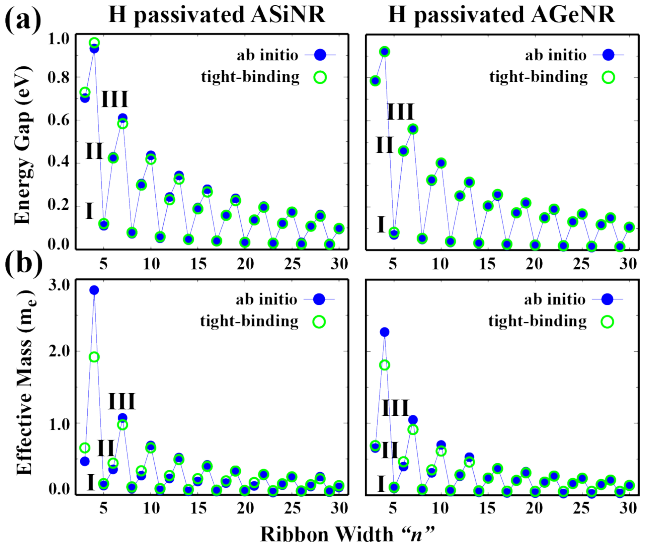

FIG. 3. Calculated (a) energy gap and (b) effective mass versus ribbon width, n, for hydrogen saturated Si and Ge armchair nanoribbons. Filled circles indicate the *ab initio* results while empty circles stand for the results of the tight binding fitting. The fitting is performed using only the energy gap data. Parameters found from this fitting was used to generate the tight binding effective mass data. In each panel three branches are observed and named in increasing order of band gaps and effective masses as family I, II, and III.

is apparently smaller at the edges, which implies that edge bonds are stronger. That is why, defining a different hopping parameter at the edges reflects the nature of the system better. Accordingly, we set the nearest neighbor hoping integrals to be $t(1+\delta)$ at the edges and t otherwise. In our model all self energies were set to zero. The tight binding parameters were obtained by fitting to the first principles results. Results presented in Fig.3 (a) show that the model used here is successful in reproducing the DFT band gap trends of both Si and Ge armchair nanoribbons. Since we did not make GW correction to the band gaps, the nearest neighbor hopping integrals, which are found to be $t = 1.03$ eV for Si and $t = 1.05$ eV for Ge, are expected to have larger values and should be taken as a qualitative result. However, the relative increase of the hopping integrals at the edges defined by δ can be taken as a quantitative result. We have found $\delta = 0.12$ and $\delta = 0.08$ for Si and Ge, respectively. Interestingly, the value found for Si is equal to that of reported value for the armchair graphene nanoribbons. To sum up, the tight binding parameters determined for Si and Ge armchair nanoribbons are $t_{Si} = 1.03$ eV, $t_{Ge} = 1.05$ eV, $t_{Si,edge} = 1.15$ eV and $t_{Ge,edge} = 1.13$ eV.

Figure 3 (b) presents the effective masses of the first conduction band calculated by using the formula

$$m^* = \hbar^2 \left(\frac{\partial^2 E(k)}{\partial k^2}\right)^{-1} \quad (1)$$

where $E(k)$ is calculated by using both DFT and tight